

# Ab initio calculations of optical properties of silver clusters: Cross-over from molecular to nanoscale behavior

John T. Titantah<sup>1</sup> and Mikko Karttunen<sup>1</sup>

Department of Mathematics and Computer Science & Institute for Complex Molecular Systems, Eindhoven University of Technology, P.O. Box 513, MetaForum, 5600 MB Eindhoven, the Netherlands

Received: date / Revised version: date

**Abstract.** Electronic and optical properties of silver clusters were calculated using two different *ab initio* approaches: 1) based on all-electron full-potential linearized-augmented plane-wave method and 2) local basis function pseudopotential approach. Agreement is found between the two methods for small and intermediate sized clusters for which the former method is limited due to its all-electron formulation. The latter, due to non-periodic boundary conditions, is the more natural approach to simulate small clusters. The effect of cluster size is then explored using the local basis function approach. We find that as the cluster size increases, the electronic structure undergoes a transition from molecular behavior to nanoparticle behavior at a cluster size of 140 atoms (diameter  $\sim 1.7$  nm). Above this cluster size the step-like electronic structure, evident as several features in the imaginary part of the polarizability of all clusters smaller than  $\text{Ag}_{147}$ , gives way to a dominant plasmon peak localized at wavelengths  $350 \text{ nm} \leq \lambda \leq 600 \text{ nm}$ . It is, thus, at this length-scale that the conduction electrons' collective oscillations that are responsible for plasmonic resonances begin to dominate the opto-electronic properties of silver nanoclusters.

**PACS.** 61.46.Df Structure of nanocrystals and nanoparticles – 36.40.-c Atomic and molecular clusters

## 1 Introduction

The readiness with which noble metal nanoparticles create and support surface plasmons makes them useful in a wide range of applications, e.g., in photonic devices, as chemical sensors [1, 2, 3, 4, 5], in bio-imaging [6], in drug delivery [7], cancer therapy [7, 8, 9], optical manipulation [10, 11, 12, 2], electrical conduits in microelectronic industry [13, 14, 15], and even as 'nanoeears' in optical readout of acoustic waves generated in liquid media [16] and in channeling photon energy in vortex nanogear transmission [17].

The changing electronic and optical properties of these materials with size from molecular clusters through nanometer scale to micrometer range and their morphology govern their domain of applicability. However, the properties of the sub-10 nm end of these noble metals, for which quantum effects become crucial [18], is not well studied although this end is of great importance for biological applications. Beyond this range theoretical studies of the optical properties are usually conducted based on classical electrodynamic approaches. Medium sized clusters (20-500 atoms) have scarcely been investigated, whereas at this size scale intriguing behaviors have been reported. For instance, Yuan and coworkers observed an unexpected luminescence change during the purification of thiolate-protected  $<2$  nm Ag nanoclusters; the non-luminescent Ag nanocluster became highly luminescent when passed through a separation column [19]. Full quantum investi-

gations are often limited to few atoms clusters. These involve tight-binding calculations [20, 21, 22], and the time-dependent density functional theory (TDDFT) approach [22]. A promising atomistic method that can be conveniently used on hundreds of atom systems is the capacitance-polarizability interaction model [23, 24] which has been successfully used to study the effect of planar defects on the optical properties of Ag nanostructures [25]. Those based on the classical electrodynamic theory of a dielectric object in an electromagnetic field use methods such as the Mie theory [26, 27], the discrete dipole approximation [28, 29] and the finite-difference time-domain approaches. Optical forces are also often computed using the Maxwell stress tensor [30, 27]. All these classical electrodynamic studies exploit the frequency-dependent dielectric constant of the bulk materials, the size dependence of these dielectric constants being extrapolated through the size dependence of the life-time broadening  $\gamma = Av_F/R$  which requires the knowledge of the Fermi velocity  $v_F$  of the bulk metal. The lower limit of the dimensions of the nanoparticle that this extrapolation may apply to is dictated by the electron mean free path in the bulk system of  $\sim 57$  nm [31]. A thorough DFT study on spherical Ag clusters of sizes ranging from 0.4 to 2 nm have found that the plasmon frequency becomes size-dependent and that the collision frequency  $\gamma$  has a more complex dependence on the particle radius [3] than the usual  $1/R$  dependence. Because of this limitation, the usual size-dependent Drude-

model may not be applicable to small nanoparticles where quantum confinement of the electrons become very important [18], and certainly may not help in understanding the mechanism governing the optical properties of nanoparticles and clusters.

In this work, we use two quantum mechanical approaches to calculate the complex permittivity of Ag clusters with sizes ranging from few atoms to hundreds of atoms. The two methods used are 1) the all-electron full-potential linearized-augmented plane-wave [32] and 2) local basis function DFT approach [33,34]. The latter has been used to predict the half-metallic character of graphene nanoribbons [35] and to probe the optical properties of armchair graphene nanoribbons embedded in hexagonal boron nitride lattices [36]. The local basis function approach is adopted for further studies due to its simplicity and robustness.

## 2 Methods

We used the WIEN2K all-electron-full-potential linearized-augmented plane-wave (LAPW) code [32], with the generalized gradient approximation (GGA) [37] for the exchange and correlation potential, to calculate the electronic and optical properties of Ag clusters. In this method, the system is described by a 3D periodically repeated unit cell which is partitioned into non-overlapping muffin-tin spheres centered on each atom and interstitials. The Kohn-Sham wave function is described as a linear combination of atomic basis functions in the muffin-tin spheres and as plane-waves in the interstitials. Muffin-tin radii of 1.3 Å around the Ag atoms are used. The multipolar Fourier expansion of Weinert *et al.* [38] is used to compute the Coulomb potential. Using the LAPW method, the cluster of interest is positioned at the center of a cubic unit cell with sides larger than the diameter of the cluster. The limit of isolated cluster cannot be reached using this approach since (strictly speaking) infinitely large unit cell is required and the computation in empty space becomes prohibitive for large unit cells; this method can only give trends towards isolated clusters. Two parameters govern the accuracy of the calculations: 1) The product of the plane-wave cut-off and the smallest muffin-tin radius in the system ( $RKM$ ), and 2) the number of  $k$ -points in the irreducible Brillouin zone (IBZ). For these clusters,  $RKM$ -value of 5.5 is sufficient to yield converged optical properties. We use 4  $k$ -points in the IBZ for the self-consistent calculations, and 20 for calculations of optical properties.

We also employed a second method, a local basis function approach within the generalized gradient approximation of the exchange and correlation energy of Perdew, Burke and Wang [37] as implemented in the SIESTA code [33,34]. In this method the basis functions are made to vanish beyond a predefined cut-off distance. For clusters, a multi-grid approach was used to calculate the electrostatic potential in accordance with the range of the lower moments of the charge density. This approach is particularly appropriate for large clusters as it scales linearly with

the number of atoms in the cluster. The core-electrons are described by the Troullier-Martins norm conserving pseudopotential [39]. The  $4d^{10}5s^1$  electrons are considered as the valence electrons for Ag. The double- $\zeta$  (DZ) basis set [40] (each occupied orbital is described by two basis functions) is used to represent the valence states. No polarization function was used as attempts to include it did not improve the results. With LAPW, periodic boundary conditions were applied. The SIESTA calculations did not use them.

For the LAPW approach optical properties were obtained from the joint density of states modified with the respective dipole matrix elements [41]. The SIESTA code computes the imaginary part of the dielectric function using the linear response function [42]:

$$\epsilon_2(\omega) = \frac{1}{4\pi\epsilon_0} \left( \frac{2\pi e}{m\omega} \right)^2 \sum_{\mathbf{k}} |\mathbf{p}_{c,v}|^2 \delta(E_c(\mathbf{k}) - E_v(\mathbf{k}) - \hbar\omega) \times [f(E_v(\mathbf{k})) - f(E_c(\mathbf{k}))], \quad (1)$$

where the subscripts  $v$  and  $c$  represent the valence and conduction bands, respectively,  $\hbar\omega$  the photon energy,  $m$  the electron mass,  $E_{c,v}(\mathbf{k})$  the conduction and valence band energies with  $k$ -vector  $\mathbf{k}$ , and  $\mathbf{p}_{c,v}$  is the momentum operator.  $f$  is the Fermi function and  $\delta$  is the Dirac delta function. The real part of the dielectric function was obtained by using the Kramers-Kronig relation

$$\epsilon_1(\omega) = 1 + \frac{2}{\pi} P \int_0^\infty \frac{\omega' \epsilon_2(\omega')}{\omega'^2 - \omega^2} d\omega', \quad (2)$$

where  $P$  stands for the Cauchy principal value.

Relaxed clusters were used for studying optical properties. Relaxation was performed as follows: Each cluster was cut out from an FCC structure and pre-relaxed using a molecular dynamics (MD) run by using a recently parameterized many-body Gupta potential for Ag [43]. The MD relaxation was performed at 300 K with the temperature kept constant using the Nosé-Hoover thermostat [44, 45]. The resulting structures were further relaxed using the SIESTA code [33,34] via the conjugate gradient method. The DFT fine-tuning was continued until forces on all atoms became smaller than 40 meV/Å.

## 3 Results

### 3.1 Comparison between local basis function and plane wave methods

He and Zeng [46] used the SIESTA code [33,34] to calculate the optical properties of Ag clusters with sizes ranging from 13 to 586 atoms and noted the need to scissor-shift their spectra by a fixed energy of 1.28 eV to align with experimental results; when comparing different computational results, it is important to notice that the magnitude of the shift needed to align with experiments depends on the exchange correlation functional. The need to apply a scissor-shift is a consequence of the well-known underestimation of the band-gap by the single particle DFT

approach [47,48,46]; techniques that contain the missing many-body effect like the GW (BSE) approach [49,48] cannot be used with large system sizes such as here, since the computational cost scales as  $N^4$ , where  $N$  is the number of electrons in the system.

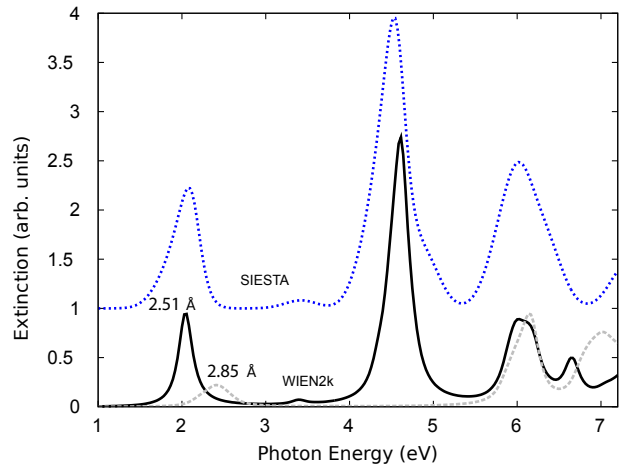
Since one of the aims here is to compare the applicabilities of the two different approaches, the results presented in this work do not include any shift except for  $\sim 0.3$  eV blue-shift to the WIEN2k data to align with the SIESTA results for easier comparison. Our calculations of the extinction coefficient of the Ag dimer ( $\text{Ag}_2$ ) revealed four major features within the energy range of 1-7 eV, Fig. 1. All optical peaks are well reproduced by both methods apart from a global redshift of about 0.3 eV of the WIEN2k results with respect to the SIESTA ones. This shift is most likely a consequence of the periodic boundary conditions in the WIEN2K simulations (a cubic unit cell with side length of 10 Å). The equilibrium dimer bond length of 2.51 Å was found, which compares very well with the measured value of 2.53 Å [50] and another computed value of 2.52 Å [51].

Two of the features (at 1.8-2.4 eV and 4.3 eV) are sensitive to the Ag-Ag bond length: A computation using a relatively long dimer bond length of 2.85 Å is seen to affect these features, Fig. 1. These features may be responsible for the widely varying optical spectra [52] of Ag nanoclusters consisting of only a few atoms since such small clusters may have a wide variation in bond lengths. The optical features of  $\text{Ag}_2$  dimer found here are consistent with the density of states (DOS) calculation of Pereiro *et al.* [53]; the imaginary part of the dielectric constant is proportional to the valence- and conduction-band joint density of states. The minor feature at 3.5 eV is again reproduced by both techniques.

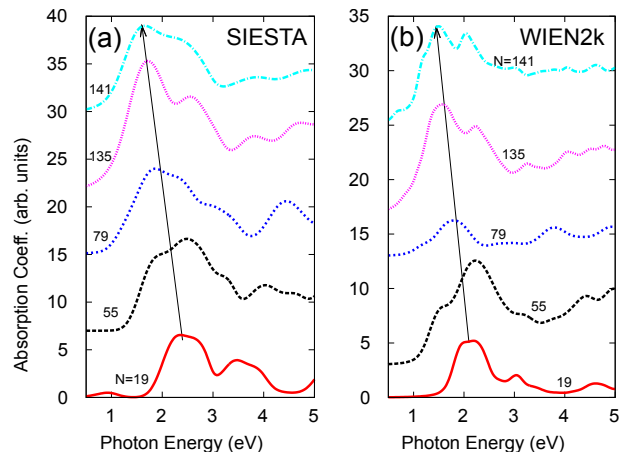
The robustness of SIESTA approach is further demonstrated by the optical absorption of triangular  $\text{Ag}_3$  that yields four features at 320-350, 360-390, 430-460 and 460-500 nm. These numbers compare well with the experimental values of 320-330, 380-390, 410-420 and 480-490 nm as reported in Ref. [54]. Next, we compare the absorption coefficients for medium sized clusters.

Figure 2 shows the absorption coefficient on a series of Ag clusters with size ranging from 19 to 141 atoms. The methods compare well with each other in terms of the peak positions (aside from a global redshift of 0.3 eV of the WIEN2k spectra with respect to the SIESTA's) and the relative heights of the peaks. The results for  $\text{Ag}_{55}$  compare very well with measured UV-photoelectron spectra on  $\text{Ag}_{55}^-$  [55], apart from the global shift to lower photon energy of 1.3 eV (practically the value of the scissor-shift of 1.28 eV reported by He and Zeng [3]). Both the position and relative intensities of the four features within 5 eV agree well with UV-photoelectron data. The comparison appears even better than with very recent TDDFT calculations [56].

As the next step, we had an  $\text{Ag}_{55}$  dimer at varying separations ranging from touching to about 10 nm. Figure 3(a) reveals a transition from a sharp to a broad resonance. This is very similar to the experimentally re-



**Fig. 1.** Comparison of the extinction coefficient of  $\text{Ag}_2$  calculated using the SIESTA and the WIEN2k codes. All optical peaks are well reproduced by both methods apart from a global redshift of about 0.3 eV of the WIEN2k results with respect to the SIESTA one. Thus the WIEN2k spectrum has been shifted by 0.3 eV to align with local basis function calculations. For WIEN2k, we show results for two dimer bond lengths of 2.51 Å (black) and 2.85 Å (light grey) while the SIESTA result is given only for the equilibrium dimer bond length of 2.51 Å.



**Fig. 2.** Absorption coefficients. Lines: Tendency of the absorption onset to shift to lower energies as cluster size increases.

ported transition when an array of 100 nm Ag nanoclusters embedded into poly (dimethylsiloxane) (PDMS) was stretched to increase the inter-particle separation [57]. This transition was attributed to quadrupolar interactions which dominate for such large nanoparticles. Quadrupolar interactions are, however, negligible for the cluster sizes considered here. This indicates that dipolar interactions also contribute to this effect.

In the LAPW approach which uses periodic boundary conditions within a cubic unit cell, the size of the unit cell determines the inter-cluster distance. On increasing the unit cell size for the  $\text{Ag}_{55}$  calculation (equivalent to increasing inter-cluster separation), we find that the same trend of transition from a sharp to a broad resonance, as found using SIESTA (see Fig. 3A), is also present in

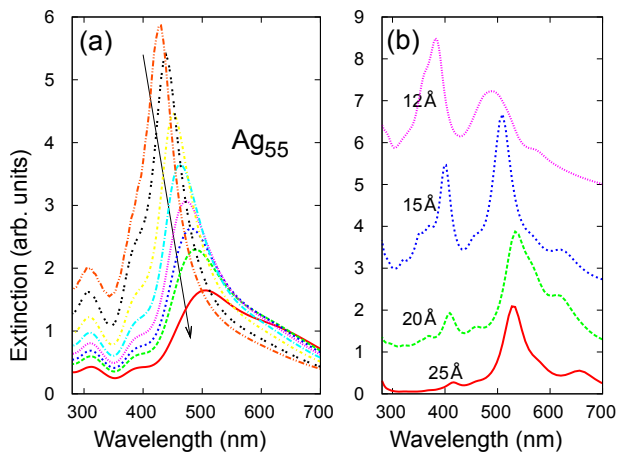


**Fig. 3.** Extinction coefficient of  $\text{Ag}_{55}$  dimers as obtained from a) SIESTA code and b) a 3D array of  $\text{Ag}_{55}$  clusters using WIEN2k for various unit cell sizes ranging from 12 Å to 25 Å. The arrow points towards increasing dimer separation from touching (center-to-center distance of 13 Å) to well separated clusters ( $>10$  nm). In b) notice that as the unit cell size increases, the intensity of the peak at 370-400 nm vanishes while that at 500 nm increases.

the WIEN2k results. For example, as the unit cell size increases from 1.2 to 2.5 nm, the feature at 370 nm diminishes and eventually vanishes leaving a single peak which shifts from 480 to 520 nm as seen in Fig. 3B.

The redshift in the plasmon resonance frequency with increasing particle separation is also in agreement with experiments [58] and theoretical calculations based on the discrete dipole approximation on dimers [59]. Our results also confirm that the plasmon resonance becomes narrower with increasing cluster size as will be shown later [60]. We also studied the effect of unit cell size on the extinction coefficient of  $\text{Ag}_{19}$  ( $2R \sim 1$  nm). For large unit cells ( $2R/L < 1/2$ ), using WIEN2k, the spectrum is characterized by a single dominant feature at about 530 nm. But for small unit cells a second peak appears at a shorter wavelength which may indicate the appearance of conductive overlap [61] between even such small clusters.

The above results show that both the SIESTA and WIEN2k approaches yield qualitatively similar optical properties. Considering the good agreement between the two methods, we use the local basis function method in further studies below.

### 3.2 Plasmon energy and cluster size

Using the SIESTA code, complex polarizability  $\alpha$  was calculated for cluster sizes ranging from 55 to 369 atoms, Fig. 4. The Clausius-Mossotti polarizabilities were calculated using

$$\alpha(\omega) = \frac{3d^3}{4\pi} \frac{\epsilon(\omega) - \epsilon_0}{\epsilon(\omega) + 2\epsilon_0}, \quad (3)$$

where  $d$  is the size of the cluster,  $\epsilon_0$  the dielectric constant of the surrounding medium and  $\epsilon(\omega)$  is the frequency dependent complex dielectric constant of the cluster. The

plasmon resonances show a crossover which appears at the cluster size of about 140. For  $N < 140$  the molecular character shows up as multiple features in the imaginary part of the polarizability of smaller clusters. For example, the two features at  $\sim 3$  eV and 3.5 eV in the imaginary part of the polarizability of  $\text{Ag}_{87}$  and  $\text{Ag}_{135}$  merge into one at 3-3.5 eV for clusters above 140 atoms. For the smaller  $\text{Ag}_{55}$  cluster, the skewed shape of the imaginary part of the polarizability is a sign of more than one feature in the optical spectrum. For clusters larger than  $\text{Ag}_{135}$  only one symmetric feature, the plasmon peak, can be seen.

The cluster size at which this crossover is found is similar to that reported for  $<2$  nm Ag nanoclusters [19]. For  $N > 140$ , the molecular transitions give way to nanometallic single optical transition energy which is characteristic of s-electrons excitations of the noble metal. This finding is in excellent agreement with TDDFT computations of Weissker *et al.* who found a cross-over from multi-feature optical spectrum of Ag clusters as the size increases above 140 atoms [62]. It is also in good agreement with a recent UV/VIS study on silver clusters protected with 2-phenylethanethiol (PET), 4-fluorothiophenol (4-FTP) and (4-(t-butyl)benzenethiol (BBS) which found the emergence of metallicity in Ag clusters composed of 150 atoms [63]. We also find that the optical transitions redshift as the cluster size increases. The tendency of redshifting with increasing cluster size is also evident in the WIEN2K results, Fig. 2b. This redshift has also recently been reported for glutathione-stabilized magic numbers (15, 18, 22, 25, 29 and 38) 1-2.5 nm Ag clusters [64] whereby a peak-edge onset of 2.1 eV for  $\text{Ag}_{15}$  was found. This agrees with the value of 2.3 eV (530 nm) that we found for  $\text{Ag}_{19}$ . Recent studies using surface second harmonic generation spectroscopy [65] and manufactured highly fluorescent Ag nanoclusters in alumina-silica composite optical fiber [66] also found redshift with increasing cluster size. Similar redshift has also been found for Au clusters [67]. The observation of redshift with increasing cluster size for small nanoclusters (where higher multipoles than dipole effects are absent) as the ones studied here, indicates that the increasing importance of higher multipole effects with increasing nanoparticle size is not enough to explain alone the redshift as has been previously suggested [68].

### 3.3 Effect of cluster shape on the optical properties

In order to understand the effect of shape change on the optical behavior of Ag clusters, we elongated an almost spherical  $\text{Ag}_{369}$  cluster into an almost elliptical one. The resulting structures were relaxed using DFT and the optical properties were evaluated. Figure 5 shows the wavelength dependence of the optical absorption of these deformed clusters. The approximate major to minor axis ratio is denoted by  $R^{\text{maj}/\text{min}}$ . For large nanoparticles, we would expect the optical properties to become anisotropic, with each optical spectrum revealing two absorption modes as the cluster adopts cigar or rod-like shapes: Longitudinal (low energy) and transverse (high energy) modes. The calculated optical absorption of  $\text{Ag}_{369}$ , for  $R = 1^{\text{maj}/\text{min}}$

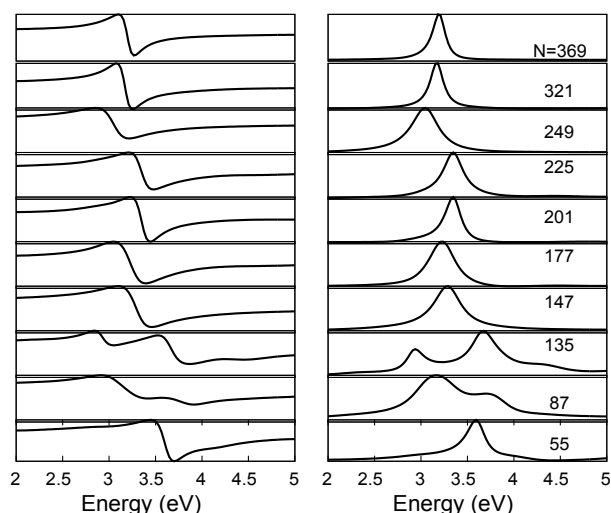


**Fig. 4.** Cluster size effect on the complex polarizability of Ag clusters for cluster sizes ranging from 55 to 369 atoms. The real part is shown in the left and the imaginary in the right. Note that for clusters smaller than  $\text{Ag}_{147}$ , the imaginary part has more than one optical feature - a signature of molecular character.

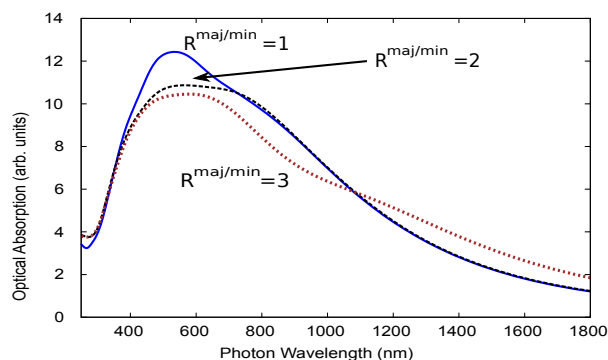


**Fig. 5.** The optical absorption of spherical and elliptical Ag clusters. The aspect ratio  $R^{\text{maj}/\text{min}}$  of the clusters of similar number of atoms  $\text{Ag}_{369}$  are indicated as approximate ratio of the principal to the minor axis.

clearly shows two features: One at 500 nm and the other at about 800 nm, revealing a not-so-spherical shape. The latter wavelength falls well within reported values of 700–1100 nm for the longitudinal plasmon resonance of Ag nanorice (rounded nanobars) [69]. Upon deforming further this structure to get an approximate aspect ratio of  $R^{\text{maj}/\text{min}} = 2$ , the intensity of the 500 nm feature reduces and broadens, and the wavelength of the peak at 800 nm only slightly increases. At an aspect ratio of about 3 a major shift in the longitudinal mode to a longer wave length of  $\sim 1100$  nm is obtained. This clearly indicates that even at such particle sizes, shape plays a crucial role for localized surface plasmons of Ag clusters. However, of the three structures of  $\text{Ag}_{369}$  studied here, the ground state energy of the undeformed is the lowest, clearly showing that small clusters prefer spherical shapes.

## 4 Summary

Two different DFT approaches were used to compute the optical and electronic properties of small and medium sized Ag clusters with reasonable agreement between them. Not surprisingly, the local basis function approach using SIESTA code turned out to be more appropriate for optical properties of Ag nanoclusters and it provides a very good description of their structural properties. Using this method, we locate a cross-over to nanoscale behaviour at the size of 140 atoms. At this size, the electronic properties of Ag clusters change from molecular character (discrete transition energies) to a nanoparticle behavior characterized by a single plasmon resonance frequency. We demonstrated the tendency of redshifting when clusters begin to agglomerate to form composite structures.

The results of the local basis function DFT computations demonstrate the power of the approach and its potential in understanding the structural, energetic, electronic and optical properties of technologically relevant noble metal nanoparticles and their derivatives.

## Acknowledgments

We thank Björn Baumeier for critical reading of the manuscript. The initial part of this work was supported by the Natural Sciences and Engineering Research Council of Canada (MK).

## References

1. Y.Q. Chen, C.J. Lu, *Sens. Actuators B Chem.* **135**, 492 (2009)
2. E. Filippo, A. Serra, D. Manno, *Sens. Actuators B Chem.* **138**, 625 (2009)
3. X. He, C. Hu, H. Liu, G. Du, Y. Xi, Y. Jiang, *Sens. Actuators B Chem.* **144**, 289 (2010)
4. M.R.H. Nezhad, J. Tashkhourian, J. Khodaveisi, *J. Iran. Chem. Soc.* **7**, S83 (2010)
5. R.F. Ngece, N. West, P.M. Ndingili, R.A. Olowu, A. Williams, N. Hendricks, S. Mailu, P. Baker, E. Iwuoha, *Int. J. Electrochem. Sci.* **6**, 1820 (2011)
6. V.V. Kravets, K. Culhane, I.M. Dmitruk, A.O. Pinchuk, *Glycine-coated photoluminescent silver nanoclusters*, in *Colloidal Nanocrystals for Biomedical Applications VII*, edited by W. Parak, K. Yamamoto, M. Osinski (SPIE, 2012), Vol. 8232 of *Proceedings of SPIE*, ISBN 978-0-8194-8875-6
7. N. Portney, M. Ozkan, *Anal. Bioanal. Chem.* **384**, 620 (2006)
8. X. Huang, I. El-Sayed, W. Qian, M. El-Sayed, *J. Am. Chem. Soc.* **128**, 2115 (2006)
9. M.M. Shenoj, I. Iltis, J. Choi, N.A. Koonce, G.J. Metzger, R.J. Griffin, J.C. Bischof, *Molec. Pharmaceutics* **10**, 1683 (2013)
10. A. Ashkin, *Phys. Rev. Lett.* **24**, 156 (1970)
11. A. Ashkin, J.M. Dziedzic, J.E. Bjorkholm, S. Chu, *Optics. Lett.* **11**, 288 (1986)

12. M. Liu, T. Zentgraf, Y. Liu, G. Bartal, X. Zhang, *Nature Nanotechnol.* **5**, 570 (2010)
13. D. Chen, X. Qiao, X. Qiu, J. Chen, *J. Mater. Sci.* **44**, 1076 (2009)
14. S.L.C. Hsu, R.T. Wu, *Mater. Lett.* **61**, 3719 (2007)
15. H. Lee, K. Chou, Z. Shih, *Int. J. Adhes. Adhes.* **25**, 437 (2005)
16. A. Ohlinger, A. Deak, A.A. Lutich, J. Feldmann, *Phys. Rev. Lett.* **108** (2012)
17. S.V. Boriskina, B.M. Reinhard, *Nanoscale* **4**, 76 (2012)
18. J.A. Scholl, A.L. Koh, J.A. Dionne, *Nature* **483**, 421 (2012)
19. X. Yuan, Q. Yao, Y. Yu, Z. Luo, X. Dou, J. Xie, *J. Phys. Chem. Lett.* **4**, 1811 (2013)
20. F. Bassani, M. Bourg, F. Cocchini, *II Nuovo Cimento D* **5**, 419 (1985)
21. A. Bfone, F. Bassani, *Z. Phys. D* **29**, 73 (1994)
22. R.W. Burgess, V.J. Keast, *J. Phys. Chem. C* **115**, 21016 (2011)
23. J. Kongsted, A. Osted, L. Jensen, P. Astrand, K. Mikkelsen, *J. Phys. Chem. B* **105**, 10243 (2001)
24. L.L. Jensen, L. Jensen, *J. Phys. Chem. C* **113**, 15182 (2009)
25. X. Ben, P. Cao, H.S. Park, *J. Phys. Chem C* **117**, 13738 (2013)
26. G. Mie, *Ann. Phys. (Leipzig)* **25**, 377 (1908)
27. V.D. Miljkovic, T. Pakizeh, B. Sepulveda, P. Johansson, M. Kall, *J. Phys. Chem. C* **114**, 7472 (2010)
28. B.T. Draine, *Astrophys. J.* **333**, 848 (1988)
29. B.T. Draine, P.J. Flatau, *J. Opt. Soc. Am. A Opt. Image Sci. Vis.* **11**, 1491 (1994)
30. K. Okamoto, S. Kawata, *Phys. Rev. Lett.* **83**, 4534 (1999)
31. H. Xu, *Appl. Phys. Lett.* **87**, 066101 (2005)
32. P. Blaha, K. Schwarz, P. Sorantin, S.B. Trickey, *Comput. Phys. Commun.* **59**, 399 (1990)
33. D. Sanchez-Portal, P. Ordejon, E. Artacho, J. Soler, *Int J Quantum Chem* **65**, 453 (1997)
34. J. Soler, E. Artacho, J. Gale, A. Garcia, J. Junquera, P. Ordejon, D. Sanchez-Portal, *J. Phys. Condens Matter* **14**, 2745 (2002)
35. Y.W. Son, M.L. Cohen, S.G. Louie, *Nature* **444**, 347 (2006)
36. H. Nematian, M. Moradinasab, M. Pourfath, M. Fathipour, H. Kosina, *J. Appl. Phys.* **111**, 093512 (2012)
37. J. Perdew, K. Burke, Y. Wang, *Phys. Rev. B* **54**, 16533 (1996)
38. M. Weinert, E. Wimmer, A.J. Freeman, *Phys. Rev. B* **26**, 4571 (1982)
39. N. Troullier, J.L. Martins, *Phys. Rev. B* **43**, 1993 (1991)
40. E.R. Davidson, D. Feller, *Chem. Rev.* **86**, 681 (1986)
41. C. Ambrosch-Draxl, J.A. Majewski, P. Vogl, G. Leising, *Phys. Rev. B* **51**, 9668 (1995)
42. P.T. Yu, M. Cardona, *Fundamentals of Semiconductors: Physics and Materials Properties* (Springer, Berlin, 2001)
43. J.T. Titantah, M. Karttunen, *Eur. Phys. J. B* **86**, 288 (2013)
44. S. Nosé, *Mol. Phys.* **52**, 255 (1984)
45. W.G. Hoover, *Phys. Rev. A* **31**, 1695 (1985)
46. Y. He, T. Zeng, *J. Phys. Chem. C* **114**, 18023 (2010)
47. J.P. Perdew, *Int. J. Quantum Chem.* **19**, 497 (1985)
48. M.S. Hybertsen, S.G. Louie, *Phys. Rev. B* **34**, 5390 (1986)
49. L. Hedin, *Phys. Rev.* **139**, A796 (1965)
50. B. Simard, P. Hackett, A. James, P. Langridgesmith, *Chem. Phys. Lett.* **186**, 415 (1991)
51. R.L. Martin, *J. Chem. Phys.* **86**, 5027 (1987)
52. J.C. Idrobo, W. Walkosz, S.F. Yip, S. Oeguet, J. Wang, J. Jellinek, *Phys. Rev. B* **76**, 205422 (2007)
53. M. Pereiro, D. Baldomir, *Phys. Rev. A* **75**, 033202 (2007)
54. S. Fedrigo, W. Harbich, J. Buttet, *J. Chem. Phys.* **99**, 5712 (1993)
55. H. Häkkinen, M. Moseler, O. Kostko, N. Morgner, M. Hoffmann, B. von Issendorff, *Phys. Rev. Lett.* **93** (2004)
56. M. Kuisma, A. Sakko, T.P. Rossi, A.H. Larsen, J. Enko-vaara, L. Lehtovaara, T. Rantala, *Phys. Rev. B* **91** (2015)
57. D. Evanoff, G. Chumanov, *ChemPhysChem* **6**, 1221 (2005)
58. M.K. Kinnan, G. Chumanov, *J. Phys. Chem. C* **114**, 7496 (2010)
59. Q. Lin, Z. Sun, *Optik* **122**, 1031 (2011)
60. M. Sendova, M. Sendova-Vassileva, J. Pivin, H. Hofmeister, K. Coffey, A. Warren, *J. Nanosci. Nanotechnol.* **6**, 748 (2006)
61. T. Atay, J. Song, A. Nurmikko, *Nano Lett.* **4**, 1627 (2004)
62. H.C. Weissker, C. Mottet, *Phys. Rev. B* **84** (2011)
63. I. Chakraborty, J. Erusappan, A. Govindarajan, K.S. Sugi, T. Udayabhaskararao, A. Ghosh, T. Pradeep, *Nanoscale* **6**, 8024 (2014)
64. S. Kumar, M.D. Bolan, T.P. Bigioni, *J. Am. Chem. Soc.* **132**, 13141 (2010)
65. T. Luenskens, P. Heister, M. Thaemer, C.A. Walenta, A. Kartouzian, U. Heiz, *Phys. Chem. Chem. Phys.* **17**, 17541 (2015)
66. A. Halder, R. Chattopadhyay, S. Majumder, S. Bysakh, M.C. Paul, S. Das, S.K. Bhadra, M. Unnikrishnan, *Appl. Phys. Lett.* **106**, 011101 (2015)
67. J. Zheng, P.R. Nicovich, R.M. Dickson, *Annu. Rev. Phys. Chem.* **58**, 409 (2007)
68. S. Link, M. El-Sayed, *Int. Rev. Phys. Chem.* **19**, 409 (2000)
69. B.J. Wiley, Y. Chen, J.M. McLellan, Y. Xiong, Z.Y. Li, D. Ginger, Y. Xia, *Nano Lett.* **7**, 1032 (2007)